Investigation of the dielectric relaxation and the transport properties of porous silicates containing humidity

A N Papathanassiou

University of Athens, Department of Physics, Section of Solid State Physics, Greece†

Abstract. The dielectric relaxation responses of pelite, which is a porous silicate sediment containing a low content of inherent humidity, were identified and characterized by employing the experimental scheme of the thermally stimulated depolarization current (TSDC) spectroscopy. Comparative experiments were performed on dry samples. The elementary responses that compose the dielectric spectrum were recorded by applying certain sampling techniques. The dielectric relaxation spectrum consists of two low-temperature mechanisms, which are related to different modes of relaxation of water molecules. A third one is probably produced by permanent dipoles consisting of point defects in the calcium participant. Three relaxation mechanisms were sampled within the intermediate temperature region and were strongly affected by the outgassing of the pore network. They correspond to polarization processes occurring in the multi-layer shell of humidity over the surface the solid aggregates. At higher temperatures, two mechanisms were traced: the first is related to the homogeneous polarization of the specimen as charge carriers migrate within conducting territories until they are trapped at internal boundaries and the latter is described as a long-distance conduction mechanism which is enhanced by the presence of humidity. The activation energy profiles of the above-mentioned relaxation mechanisms were obtained from the analysis of the experimental signals of the thermal sampling and the partial heating schemes.

1. Introduction

The dielectric and electrical properties of porous media which are partially filled or fully saturated with liquids have attracted the interest of many investigators [1–7]. A small amount of humidity hosted by the porous space of an insulating porous matrix increases the value of the static dielectric constant of the porous system by some orders of magnitude. A picture that may represent the liquid–solid interaction is that of a thin layer of humidity which coats the solid aggregates.

Significant experiments concerning a low frequency dispersion due to the liquid–solid interaction were carried out by different researchers [4, 6, 8]. The real part of the dielectric constant was measured as a function of frequency via the standard impedance spectroscopy technique at singular temperature. The resolution of the latter scheme is too limited and fails to give a detailed profile of the elementary dielectric responses. In the present work, we employ the thermally stimulated depolarization current (TSDC) spectroscopy so as to identify and characterize the humidity related relaxation mechanisms which proceed in a silicate rich pelite accommodating an inherent quantity of water. The resolving power of the TSDC permits the identification of the mechanisms that contribute to the enhanced value of the dielectric constant and the effect of outgassing the pore space and yields the evaluation of the relaxation parameters.

† Postal address: Panepistimiopolis, GR15784 Zogratos, Athens, Greece.

2. Theory

The most common types of dielectric relaxation of an insulator are: (a) the rotation of permanent dipoles, (b) the reduction of the free charge carriers' mobility due to obstacles sited inside the matrix (i.e. dislocations, grain boundaries, interfaces separating the conductive inclusions from the matrix) and (c) the space charge formation resulting from the non-ohmic sample–electrode interface [9]. The relaxation time τ is a time constant which governs the relaxation; its temperature dependence is usually described by the Arrhenius law:

$$\tau(T) = \tau_0 \exp\left(\frac{E}{kT}\right) \tag{1}$$

where E denotes the activation energy, τ_0 is the pre-exponential factor and k is the Boltzmann constant.

The usual mode of the thermally stimulated depolarization current (TSDC) method [10] consists of polarizing the specimen at a temperature T_p for the time interval $t_p \gg \tau(T_p)$. It follows the quenching to liquid nitrogen temperature (LNT) by keeping the external polarizing field on. At the LNT, the relaxation time is practically infinite, thus, on removing the electric field, the dielectric remains polarized. Afterwards, the sample is heated at a constant rate. The time (equivalently, temperature) annihilation of the polarization produces the depolarization current, which is recorded by an electrometer connected to the sample's surface. As soon as the thermal energy becomes high enough to drive the polarized dipoles to a random orientation state, a transient electric signal is recorded, which is called a thermogram.

The rotation of non-interacting dipoles induces the depolarization current:

$$I(T) = \frac{S\Pi_0}{\tau_0} \exp\left[-\frac{E}{kT} - \frac{1}{b\tau_0} \int_{T_0}^{T} \exp\left(-\frac{E}{kT}\right) dT \right] \tag{2}$$

where Π_0 is the initial polarization of the dielectric, S is the sample's surface area which is in contact with the electrode, T_0 coincides with the LNT and b is the heating rate. The activation energy E is identical to the migration enthalpy h^m of the migrating charges which are associated with an electric dipole [11].

Each relaxation mechanism contributes to the value of the static dielectric constant by an amount $\Delta\varepsilon$, which is:

$$\Delta\varepsilon = \frac{Q}{\varepsilon_0 S E_p} \tag{3}$$

where Q is the total charge released as the polarization annihilates, ε_0 is the permittivity of free space and E_p is the intensity of the polarizing electric field. Q is obtained by integration of the TSDC peak.

Depolarization curves are obtained when the polarization mechanism is an interfacial or space charge one [12]. The relaxation time τ is usually assumed to obey the Arrhenius relation (equation (1)). The interfacial polarization is related to short-distance charge transport and may be visualized as a long-dipole relaxation. The description of the space charge polarization is too complicated. The free charge population undergoes different simultaneous processes, like space charge limited drift, diffusion, neutralization to the electrodes, creation and/or recombination of charges etc [12]. It is also probable that the transferring charges are trapped by internal obstacles (traps) distributed in the bulk. The space charge TSDC peaks are sensitive to the electrode material used, i.e. the blocking degree of the sample–electrode interface. The polarization state depends strongly upon the storage conditions and the electret's prehistory [13]. Although the competing mechanisms prohibit the construction of an analytical equation describing the space charge TSDC signal, rough approaches have been made and several

approximate space charge TSDC equations have been derived. The different approximations converge to the point that the initial edge of the space charge TSDC curve coincides to that of the non-interacting rotating dipoles [14].

2.1. Decomposition of the TSDC signal to its constituents

The capability of detecting any desired relaxation mechanism that composes the thermogram is the powerful advantage of TSDC spectroscopy. The so-called 'selectivity' is attained by selecting the proper polarization conditions and annihilating the undesirable responses. In the present work, we adopt a selective polarization technique [15, 16], which resembles the thermal sampling one [17–19]: at the temperature T_p, which is located within the temperature region where a broad peak appears, the sample is polarized for the time interval t_p. Afterwards, the polarizing field is removed and the temperature of the specimen is abruptly reduced to the LNT. By polarizing at T_p, the slow relaxation mechanisms, which activate at much higher temperatures than T_p, remain practically unpolarized. In the subsequent cooling stage, the fast relaxation mechanisms, which activate at temperatures much lower than T_p, are discharged. As a result, only the mechanisms activating in the immediate neighbourhood of T_p reach a detectable polarization state. In the subsequent heating stage, a band, which corresponds to the polarized mechanisms that survived the polarization procedure and represents a portion of the initial dispersion, is recorded.

2.2. Determination of the energy spectrum

With the exception of the family of ionic crystals with extremely low concentration of impurities, it is commonly assumed that the activation energy is not single valued but distributes normally around E_0, with distribution function [20, 21]

$$f(E) = \frac{1}{\sqrt{2\pi}\sigma} \exp\left[-\frac{(E - E_0)^2}{2\sigma^2}\right] \tag{4}$$

where σ is the broadening parameter. The total depolarization current is:

$$I(T) = \int_{-\infty}^{+\infty} f(E)I(T, E)\,\mathrm{d}E \tag{5}$$

where the term $I(T, E)$ is identical to the monoenergetic TSDC equation (see equation (2)). The non-linear least squares fit of equation (5) to the experimental data points yields the relaxation parameters E_0, σ and τ_0.

The analysis of a TSDC peak by full curve fitting prescribes a certain distribution function in the relaxation parameters, like that mentioned by equation (4). However, such a selection is rather arbitrary, so, it is preferable to derive the distribution from the experimental data. The initial part of a TSDC peak, which is characterized by single valued E and τ_0, is approximated well by an exponential decay on the inverse temperature:

$$I(T) \cong \frac{S\Pi_0}{\tau_0} \exp\left(-\frac{E}{kT}\right). \tag{6}$$

It is evident that, in the limit of the low-temperature region of the TSDC peak, the slope of the $\ln I(-1/kT)$ plot is identical to the activation energy E. Fortunately enough, the low-temperature part of distributed TSDC peaks and peaks resulting from space charge mechanisms are practically insensitive to the selection of the distribution function or to the model asserted for the space charge relaxation, respectively. For a distributed peak, the aforementioned analysis provides an estimate of the activation energy merely for the fast relaxation mechanisms. The

evaluation of the activation energy over the entire temperature region where a peak appears, we may conduct successive partial discharges of the mechanisms and analyse the data through equation (6). This experimental scheme is called the partial heating [22] and yields a set of initial rise curves, which reveals actually the temperature distribution of the activation energy. The accuracy of this method is adequate for the temperature region close to the maximum of the initial peak [12] and, therefore, the results should critically be visualized in relation to the full curve fitting results.

3. Experimental details

A cryostat operating from the LNT to 420 K was used for the TSDC experiments. The specimens were placed between the two platinum electrodes of the apparatus. The depolarization current was measured by a Keithley 617 electrometer. The heating was monitored via an Air Products temperature controller, which maintained a constant heating rate, typically 2 K min^{-1}. The output signals of the electrometer and the controller were acquired by a computer, which accommodates the proper interface.

The composition of the pelite is: 2 wt% albite $NaAlSi_3O_8$, 73 wt% quartz SiO_2, 2 wt% calcite $CaCO_3$, 3 wt% ferroan clinochlore $(MgAlCrFe)_5(SiAl)_4O_{10}OH$ and 2 wt% muscovite $(KNa)(AlMgFe)_2(Si_3Al_9)$. The porosity was about 8%. Typical dimensions of the specimens were 1 cm$^2 \times$ 1 mm.

4. Results and discussion

4.1. Relaxation mechanisms and their relaxation parameters

In figure 1 we show two thermograms recorded by using different types of electrode, but keeping the polarization conditions the same. In the MSM (metal–sample–metal) configuration the specimen is placed between the metal (platinum) electrodes of the cryostat, while, in the MISIM (metal–insulator–sample–insulator–metal) arrangement, two thin insulating foils of Teflon are placed between the sample's surface and the metal electrodes of the apparatus. A strong dispersion reaches a maximum at $T_{max} = 297$ K, when metal electrodes are employed. The signal is reduced and the maximum shifts about 20 K towards lower temperatures, when insulating electrodes are used. The sensitivity of the shape and the amplitude of the thermogram to the nature of electrodes indicates that space charge relaxation participates in the dielectric relaxation. Insulating electrodes are characterized by their notable blocking degree in relation to the metal ones. Consequently, they influence the discharge of the free moving charges, which hinder the accumulation of charge near the sample surfaces and reduces the intensity of the electric field inside the specimen [17].

In figure 2, we depict the signal recorded after the quenching of the sample from room temperature to LNT as soon as the polarizing field was applied. The high-temperature peak is suppressed and some 'knees' appear in the spectrum, indicating that different relaxations compose the thermogram. In the following, we identified the components by working in two ways: in the low-temperature region, we performed a combination of proper selection of polarization conditions and partial discharge of the undesirable mechanisms, while, in the intermediate- and high-temperature regions, we applied the thermal sampling scheme.

The low-temperature region requires a null-polarization state of the high-temperature mechanisms, for two reasons. Firstly, the high-temperature mechanisms are often strong enough to mask the low-temperature response. Secondly, recalling that the high-temperature mechanisms are usually related to the space charge formation, the effective polarization field
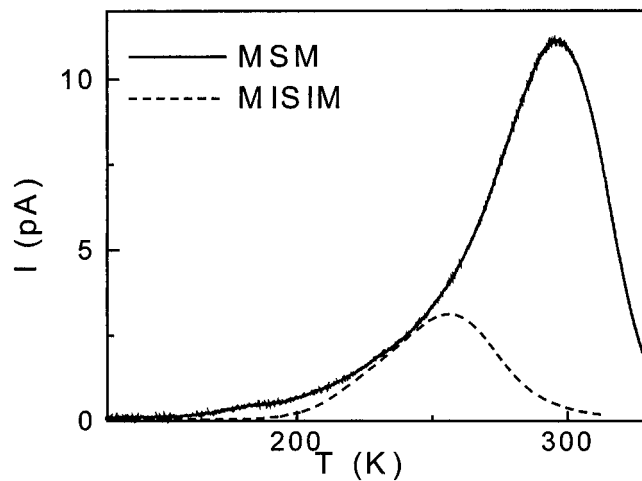
Figure 1. Thermograms obtained by employing different types of electrodes. The polarization conditions were: $T_p = 290$ K, $E_p = 2$ kV mm^{-1} and $t_p = 1$ min.
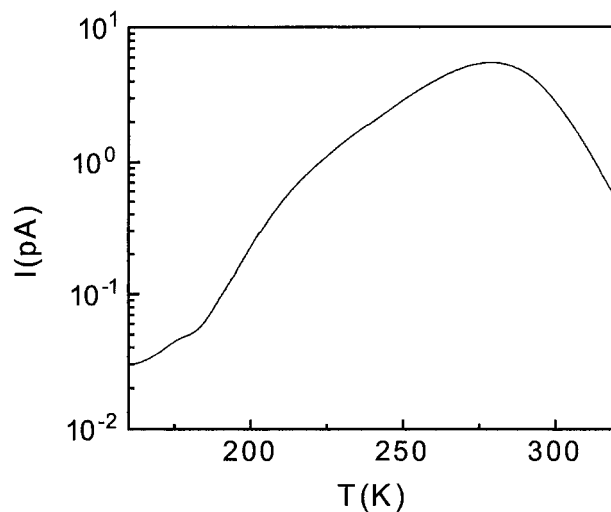

Figure 2. Identification of different overlapping mechanisms, which appear as 'knees' in the thermogram. The specimen was polarized at $T_p = 290$ K and quenched abruptly to LNT, in order to minimize the masking due to the strong high-temperature dispersion.

acting on the dipole centres is lower than that externally applied due to the accumulation of free charges toward the sample surfaces. Additionally, during the heating stage of the TSDC experiment, the relaxation of the dipoles is perturbed by the electric field produced by the inhomogeneous spatial distribution of the frozen dipole population. The key for reliable low-temperature spectroscopic investigation is the selection of the proper polarization temperature T_p. In figure 3 is the thermogram obtained by polarizing at $T_p = 180$ K for the time interval $t_p = 30$ s. Two distinct maxima appear at about 138 K and 178 K, respectively. The first mechanism (relaxation I) was individually recorded by polarizing at $T_p = 138$ K and quenching the specimen to the LNT. In the same manner, the latter dispersion (relaxation II) was polarized
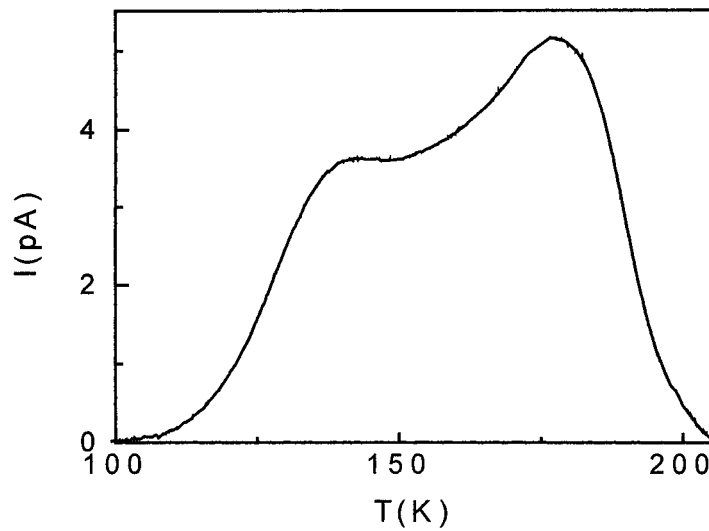
Figure 3. The low-temperature spectrum obtained by polarizing at $T_p = 180$ K for the time interval $t_p = 30$ s by an electric field of intensity $E_p = 3$ kV mm^{-1}.

Table 1. The relaxation parameters of individual dispersions, resulting from the analysis of the TSDC signals under the constraint of the normal distribution of the activation energy around a central value. The last column indicates the experimental scheme used to identify each component; details are given in the text.

	T_{max} (K)	E_0 (eV)	σ (eV)	τ_0 (s)	Decomposition scheme
I	138.0	0.196	0.019	1.454×10^{-5}	Selection of proper
II	177.6	0.267	0.008	6.667×10^{-6}	polarization
III	182.0	0.421	0.007	3.075×10^{-10}	conditions
IV	195.7	0.440	0.008	8.907×10^{-10}	in combination with
	197.0	0.441	0.009	1.036×10^{-9}	partial discharge
V	203.0	0.521	0.022	2.453×10^{-11}	
	209.0	0.525	0.025	5.540×10^{-11}	
VI	222.0	0.620	0.022	1.921×10^{-12}	
	231.5	0.622	0.020	7.659×10^{-12}	
VII	238.5	0.643	0.023	6.228×10^{-12}	Thermal sampling
	239.9	0.645	0.036	5.7234×10^{-12}	
VIII	253.5	0.651	0.035	3.199×10^{-11}	
	261.5	0.687	0.030	1.523×10^{-11}	
	267.0	0.682	0.019	3.082×10^{-11}	
	272.5	0.695	0.020	3.480×10^{-11}	
	278.0	0.700	0.036	5.511×10^{-11}	

at $T_p = 178$ K and the temperature was reduced rapidly to the LNT. However, in the subsequent heating stage, the sample was discharged up to 178 K and afterward cooled to the LNT. Then, a second run was carried out, where relaxation II is detected free from the undesirable relaxation I. The signals were analysed asserting the normal distribution of the activation energy around a mean value E_0. Equation (5) was fitted to the experimental data points. The result was visually inspected to ensure a good match in the low-temperature tail of the TSDC curve. The
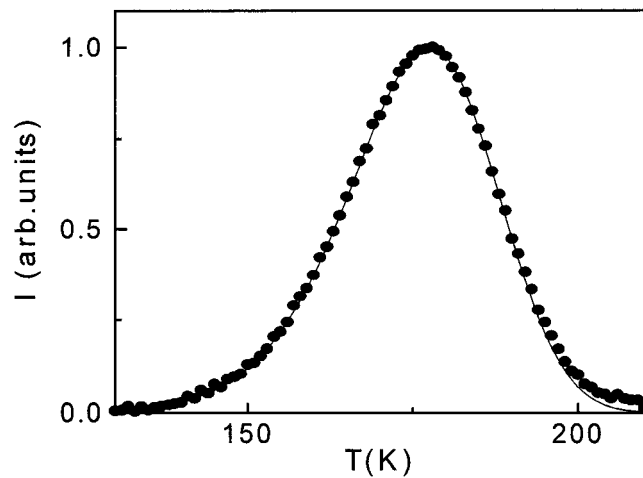
Figure 4. Comparative presentation of the normalized data points, which correspond to dispersion III, together with the theoretical curve that best matches the data points.
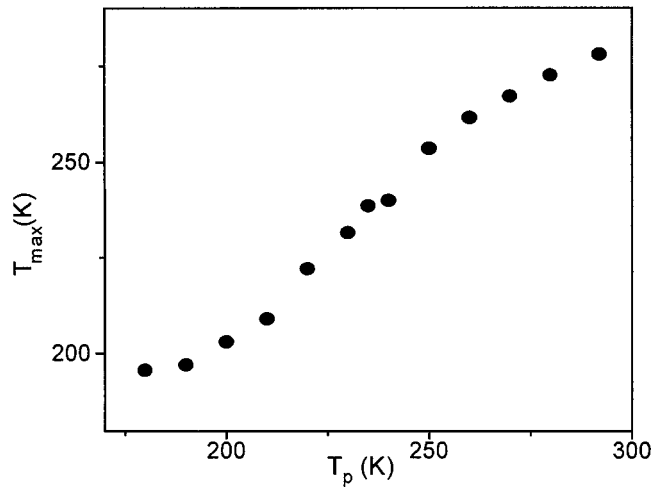

Figure 5. The temperature T_{max}, where the current reaches a maximum, of the thermal sampling responses against the polarization temperature T_p.

relaxation parameters are listed in table 1. An example for the quality of the fit is given in figure 4, where the signal of relaxation II, together with the theoretical curve that best matches the experimental data points, is depicted. The combination of the proper polarization and the partial discharge led to the identification of another relaxation mechanism with a maximum at 182 K. Its relaxation parameters were obtained asserting the normal distribution in the activation energy values (table 1).

In the intermediate- and high-temperature region, we employed the thermal sampling technique. In figure 5, the temperature distribution of the maxima of the thermal sampling responses is depicted. It is not clear if any of the data points accumulate around some T_{max} values. Therefore, the distinction between overlapping peaks is rather hard, with respect to figure 5. The signals were analysed, asserting the Gaussian distribution in the activation energy
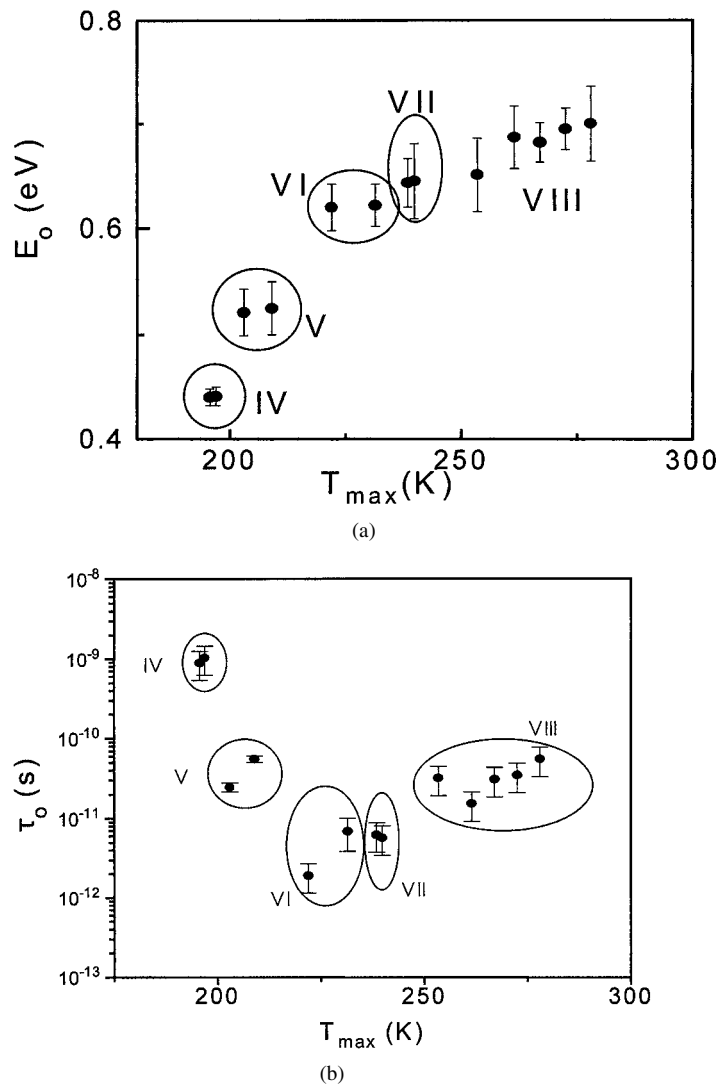
Figure 6. (a) Temperature distribution of the activation energy E_0, obtained by full-curve fitting on the thermal sampling signals. The vertical bars represent the broadening parameter σ. IV, V, VI, VII and VIII indicate the different relaxation mechanisms. (b) Temperature distribution of the pre-exponential factor τ_0, obtained by full-curve fitting on the thermal sampling signals.

values. The dependence of E_0 upon T_{max} is presented in figure 6(a), accompanied by vertical bars of length 2σ. The energy representation indicates the presence of five dispersions, labelled IV, V, VI, VII and VIII, respectively. In figure 6(b) we show the temperature distribution of the corresponding pre-exponential values. The relationship between τ_0 and E_0 is depicted in figure 7. Table 1 accommodates the relaxation parameters of dispersions IV, V, VI, VII and VIII.

Estimates of the activation energy values were obtained by analysing the signals recorded by the partial heating scheme. In figure 8 we show the activation energy values with respect to the T_c temperature, i.e. the temperature where the recording is interrupted as soon as an initial rise curve is recorded. The data points corresponding to the IV and V relaxations
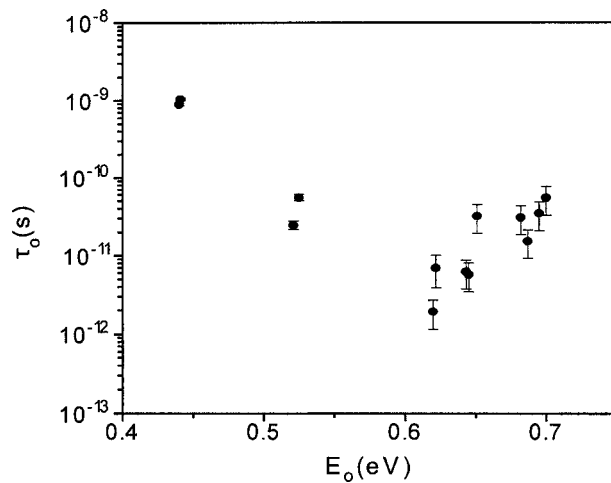
Figure 7. The pre-exponential factor τ_0 of the relaxation mechanisms recorded via the thermal sampling scheme against the central value E_0, under the constraint of normal distribution in the activation energy values.
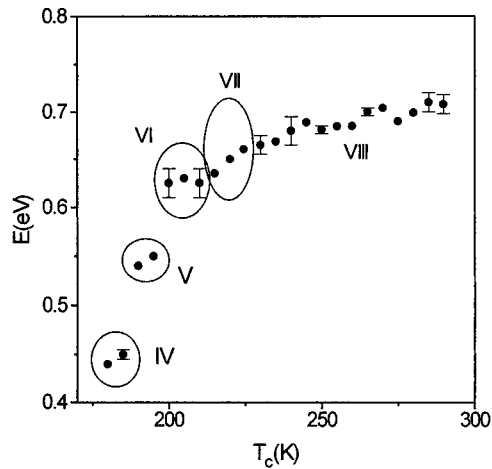

Figure 8. The activation energy E evaluated from the analysis of the partial heating scheme against the temperature T_c. Details of the experimental procedure are presented in the text.

are well defined in the diagram. Concerning the higher temperature region, it is hard to distinguish between mechanisms VI and VII, probably due to the fact that the activation energy values are closely separated. However, the energy spectrum obtained by the partial heating assists adequately well that obtained by the full-curve fitting on the thermal sampling peaks (figure 6(a)).

4.2. Effect of drying

The pore network was outgassed by placing the specimens inside a vacuum chamber at 373 K for 24 h. A turbo-molecular vacuum pump was employed so as to achieve a dynamic vacuum of about 10^{-7} bar. By weighing the samples, we found that the loss of weight was 0.07%.
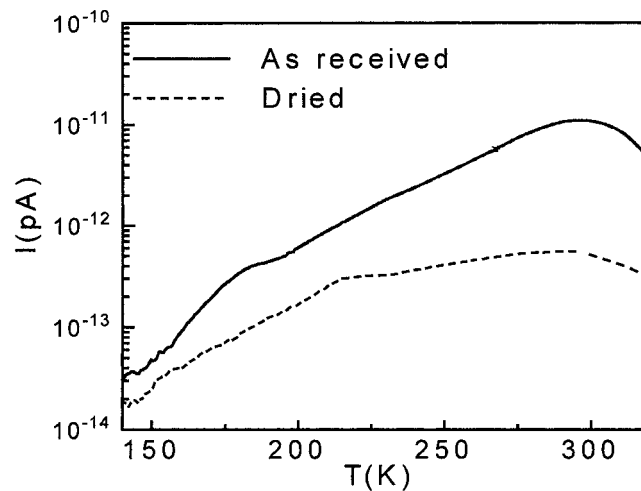
Figure 9. A thermogram obtained on an as-received sample of pelite, together with the signal recorded after the extraction of humidity from the pore network.

Table 2. Sensitivity of the relaxation mechanisms to the outgassing of the pore network. $I_{max,dry}$ and $I_{max,0}$ indicate the signal amplitude recorded on the dried sample and the as-received one, respectively.

	T_{max} (K)	$\dfrac{I_{max,dry}}{I_{max,0}}$
I	138.0	0.41
II	177.5	0.32
III	182.0	0.71
IV	195.7–197.0	0.00
V	203.0–209.0	0.10
VI	222.0–231.5	0.30
VII	238.5–239.9	0.44
VIII	RT	0.06

In figure 9, a thermogram obtained from an as-received specimen, together with another one recorded immediately after the drying procedure, are depicted in semilogarithmic presentation. The signal is reduced about one order of magnitude after the drying. In table 2, we show the percentage reduction of the amplitude for the individual relaxation mechanisms. Therein, the reduction of polarization is expressed through the ratio $I_{max,dry}/I_{max,0}$, where $I_{max,0}$ and $I_{max,dry}$ denote the signal amplitudes before and after drying, respectively. By integrating the thermogram in the time domain over the time duration of the TSDC scan, we found that the charge released is 8.5% of that emitted from the as-received specimen. Equation (3) yields the participation of the entire relaxation mechanisms detected by the TSDC spectroscopy in the value of the static dielectric constant: $\Delta\varepsilon = 21.57$ for the as-received sample and $\Delta\varepsilon = 1.83$ for the dry one.

4.3. Attribution of the relaxation mechanisms

The amplitudes of mechanisms I and II reduce to 41 and 32% of their initial amplitudes. The temperature region where the latter dispersions appear is typical for rotating dipoles, which

are either water molecules or composed of hydroxyl units [23]. The pre-exponential factors are close together (see table 1 and figure 7) indicating that a unique type of dipole (i.e. water molecules) relaxes in two different modes. The activation energy of dispersion I is much lower than that of dispersion II. Thus, the relaxing molecules which correspond to dispersion I are loosely bound to the matrix. Dispersion II corresponds to a relaxation mode of water molecules constrained by their strong bonding with the solid frame (strongly bound water).

Dispersion III is suppressed by 29% after outgassing the specimen at high temperature. Its location and behaviour after the drying provide evidence for a well known mechanism, which operates in material with calcite content [24, 25]. It is related to the rotation of point defect agglomerates, which are favoured by the calcium carbonate sublattice [23, 24, 26]. To ensure this aspect, the specimen was outgassed *at room temperature* for a long period of time, but the peak was not modified. Therefore, temperature is the only parameter that affects relaxation III in the way the thermal perturbation decomposes the defect dipole aggregates.

Peak IV eliminates after the outgassing of the pore space, while dispersions V and VI are suppressed drastically. The humidity is the most probable candidate for the aforementioned polarization mechanisms. The visualization of rotating dipoles may not demonstrate the appearance of dispersions IV, V and VI; if the polarizable entities were freely rotating water dipoles, they would induce a TSDC signal within the low-temperature region. However, dispersions IV, V and VI activate within the intermediate-temperature region, and, subsequently, they are determined by larger relaxation time. Different types of interfacial polarization within conductive inclusions can better explain the appearance of the intermediate-temperature region responses. Two different types of polarization may occur within the pore network [1, 3, 4]: one is related to the immediate location of humidity on the surface of the solid frame and another involves the subsequent hydration of the porosity. The first set of water molecules are expected to be stronger bound to the matrix than the second one, and less easily removed from the porous material. Additionally, the relaxation time for the relaxation VI, which appears at higher temperature than dispersions IV an V do, is larger than that of the latter ones, assisting the hypothesis of a strongly bound layer attached directly to the surface of the grains. Hence, dispersion VI might be related to a polarization operating in the humidity layer that is directly attached to the grains' surface, while IV and V are related to relaxation processes advancing in additional stratified layers of humidity [27].

Concerning the relaxation VII, the temperature where the current reaches a maximum is characterized by a negligible dependence upon the blocking degree of the electrode material. Dispersion VII involves the homogeneous polarization of the specimen. Charge carriers migrate along short distances in the bulk, until they are trapped by internal obstacles, like the boundaries of the grain. On the other hand, relaxation VIII is manifested as a typical space charge mechanism, due to the low reproducibility and its strong dependence on the nature of the electrodes. Its strength is significantly diminished after the drying procedure. It seems that it is related to long-distance charge transport along areas which are rich in humidity. This bulk surface conduction might proceed through the shells of humidity, which settles on the granular surface. The removal of humidity reduces the migrating paths and the proton concentration.

5. Conclusions

A small amount of humidity is responsible for the large value of the dielectric constant of as-received pelite. Different polarization mechanisms participate in the enhanced dielectric constant. We resolved and characterized the individual relaxation components of the dielectric response by different schemes of TSDC spectroscopy. The relative intensities of the low-temperature dipolar dispersions indicate that the organization of the water molecules is different

from that of freely rotating dipoles. Additionally, they are organized in a way that might be described by the interfacial polarization. Two low-temperature relaxations (I and II) were ascribed to the rotation of water molecules, which are either loosely or strongly bound to the matrix. Another dispersion III is probably attributed to defect dipoles favouring the calcium sublattice. A set of three peaks, which appear in the intermediate-temperature region, is considerably affected by the drying. They are related to the polarization of stratified shells of humidity that cover the solid grains. Among these, the one most strongly bound to the grains' surface is attributed to the direct solid–liquid interface. Finally, two more relaxation mechanisms activate close to room temperature. One is attributed to the homogeneous polarization of the specimen; charge carriers undergo a localized (short-distance) motion within conductive territories until they are trapped by inherent obstacles, such as grains' boundaries. The latter relaxation exhibits typical characteristics of space charge relaxation. Humidity enhances significantly the conduction process.

Acknowledgments

References

[1] Nettelblad B and Niklasson G A 1996 *J. Phys.: Condens. Matter* **8** 7049–58
[2] Nettelblad B 1996 *J. Appl. Phys.* **79** 7106
[3] Nettelblad B and Niklasson G A 1995 *J. Phys.: Condens. Matter* **7** L619–24
[4] Knight R and Abad A 1995 *Geophysics* **60** 431–6
[5] Endres A L and Knight R 1991 *J. Appl. Phys.* **69** 1091–8
[6] Knight R and Endres A 1990 *Geophysics* **55** 586–94
[7] Knight R and Nur A 1987 *Geophysics* **52** 644–54
[8] Chew W C and Sen P N 1982 *J. Chem. Phys.* **77** 4683
[9] Jonscher A K 1983 *Dielectric Relaxation in Solids* (London: Chelsea Dielectrics)
[10] Bucci C and Fieschi R 1964 *Phys. Rev. Lett.* **12** 16
[11] Varotsos P A and Alexopoulos K D 1985 *Thermodynamics of Point Defects and Their Relation with Bulk Properties* ed S Amelinckx, R Gevers and J Nihoul (Amsterdam: North-Holland)
[12] Vanderschueren J and Gasiot J 1979 *Field Induced Thermally Stimulated Currents in Thermally Stimulated Relaxation in Solids* ed P Braunlich (Berlin: Springer)
[13] Van Turnhout J 1975 *Thermally Stimulated Discharge of Polymer Electrets* (Amsterdam: Elsevier)
[14] Müller P 1981 *Phys. Status Solidi* a **67** 11
[15] Schrader S and Carius H-E 1991 *Proc. 7th Int. Symp. on Electrets, ISE7 (Berlin, 1991)* ed R Gerhard-Multhaupt, W Kunstler, L Brehmer and R Danz p 581
[16] Papathanassiou A N, Grammatikakis J and Bogris N 1993 *Phys. Rev.* B **48** 17 715
[17] Van Turnhout J 1980 *Thermally Stimulated Discharge of Polymers in Electrets* ed G M Sessler (Berlin: Springer)
[18] Nedetzka T, Reichle M, Mayer A and Vogel H 1970 *J. Phys. Chem.* **74** 2652
[19] Zielinski M and Kryszewski M 1977 *J. Electrostat.* **3** 69
[20] Calame J P, Fontanella J J, Wintersgill M C and Andeen C 1985 *J. Appl. Phys.* **58** 2811
[21] Laredo E, Puma M, Suarez N and Figueroa D R 1981 *Phys. Rev.* B **23** 3009
[22] Creswell R and Perlman M 1970 *J. Appl. Phys.* **41** 2365
[23] Papathanassiou A N and Grammatikakis J 1997 *Phys. Rev.* B **56** 8590
[24] Papathanassiou A N and Grammatikakis J 1996 *Phys. Rev.* B **53** 16 253
[25] Bogris N, Grammatikakis J and Papathanassiou A N 1998 *Phys. Rev.* B **58** 10 319
[26] Papathanassiou A N, Grammatikakis J, Katsika V and Vassilikou-Dova A B 1995 *Radiat. Eff. Defects Solids* **134** 247
[27] Papathanassiou A N and Grammatikakis J 2000 *Phys. Rev.* B at press